Aluminum concentration range for the extrudability of ceramic pastes

Nancy Flores-Martinez, Fabien Remondiere, Jenny Jouin, Giuseppe Fiore, Stéphane Oriol, Sylvie Rossignol

Aluminum concentration range for the extrudability of ceramic pastes

Nancy Flores-Martinez, Fabien Remondiere, Jenny Jouin, Giuseppe Fiore, Stéphane Oriol, Sylvie Rossignol

PII: S2666-5395(21)00159-0

DOI: https://doi.org/10.1016/j.oceram.2021.100213

Reference: OCERAM 100213

To appear in: *Open Ceramics*

Received Date: 31 August 2021

Revised Date: 20 December 2021

Accepted Date: 21 December 2021

Please cite this article as: N. Flores-Martinez, F. Remondiere, J. Jouin, G. Fiore, Sté. Oriol, S. Rossignol, Aluminum concentration range for the extrudability of ceramic pastes, *Open Ceramics* (2022), doi: https://doi.org/10.1016/j.oceram.2021.100213.

Graphical abstract:

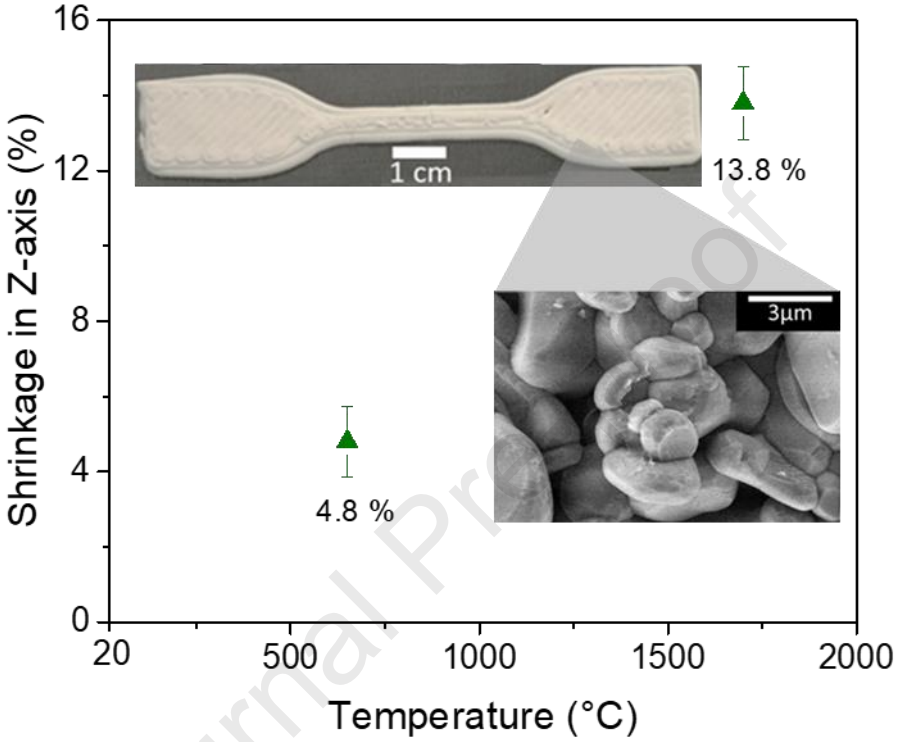

Aluminum concentration range for the extrudability of ceramic pastes

Nancy Flores-Martinez[1,2], Fabien Remondiere[1], Jenny Jouin[1], Giuseppe Fiore[2], Stéphane Oriol[2], and Sylvie Rossignol[1].

[1]Institut de Recherche sur les Céramiques, UMR 7315, 12 rue Atlantis, 87068 Limoges Cedex, France

[2]Centre National d'Etudes Spatiales, Direction des Lanceurs, 52 rue Jacques Hillairet, 75615 Paris Cedex, France

ABSTRACT

With the goal of developing refractory pastes to replace metal alloys used in turbine blades for Deep Space exploration, the French Space Agency, CNES, in collaboration with the Institute of Research for Ceramics, IRCER, has developed a preliminary research where dense alumina ceramics were formulated, printed and tested. This preliminary research will be the prelude to substituting by materials with more interesting creep properties at high temperature, for example, yttrium aluminum garnet, YAG. Since alumina is less expensive than YAG, preliminary tests were performed with alumina. These alumina pastes were 3D-printed by robocasting from very high solid loaded alumina pastes (>75 wt%), in the presence of organic additives, namely glycerol, PVA and ISOBAM 104. Several formulations of pastes were prepared, with the aim to obtain dense ceramic pieces. After, the alumina and the organic additives were mechanically mixed and the pastes were extruded with a commercial 3D printer. The best sample was obtained with a paste presenting an Al_2O_3 solid load of 79.37 wt% (63.5 vol%). A debinding step was performed afterwards to eliminate their organic content and the consolidation of the shaped pieces was finally achieved by sintering at 1700°C. A % shrinkage of 8, 6.8 and 13.8 in the X, Y and Z-axes was measured, being one of the lowest values at 1700 °C compared to those in the literature.

Keywords: alumina pastes, Al_2O_3, robocasting, Al concentration, PVA/glycerol ratio, ceramic pastes, shrinkage

1. INTRODUCTION

Advanced ceramic materials possess high temperature stability and resistance, high mechanical performance, high hardness and high resistance to corrosion[1]. The French Space Agency (CNES) has carried out research and development in oxide ceramics with the aim of improving the design of crucial subsystems for space pace propulsion[2]. The turbine maximum allowable temperature, imposed by the resistance of the metallic alloys, represents a performance limitation for Liquid Propulsion Rocket Engine cycles. The introduction of oxide ceramics for stator/rotor turbine parts could be a promising solution to increase the cycle temperature and achieve performance gains accordingly. Under a lifetime standpoint, creep-resistant ceramics could be the key technology for the development of on-board power production systems for Deep-Space exploration[2].

However, the interest in ceramic materials goes obviously beyond space applications, as they are also widely used in the magnetics[3], nuclear[4], piezoelectricity[5], medicine[6], and fuel cells[7] fields among others, all of which require specific configurations and properties. However, ceramic shaping turns out to be a major challenge[1]. In fact, the brittleness of ceramics limits the technical feasibility of their shaping by plastic deformation. Mold-dependent processes such as pressing, casting or injection molding thus shape the majority of ceramics, to mention a few[8].

Additive manufacturing (AM) or 3D printing create a final shape from a 3D model file by adding layers upon layers of material; as such, 3D technology has become one of the most versatile and customized processes applied to obtain complex ceramic parts. Some of the most developed AM techniques applied to ceramics are stereolithography[9,10], binder jetting[11,12], laminated object manufacturing[13], selective laser sintering[14,15] and extrusion free forming[16,17], the latter being one of the most widely used due to its low cost and simplicity[18]. In this

technique, the final resolution of the printed shape is directly related to the quality of the extrusion paste, which strongly depends on the ratio between its solid and liquid constituents. For example, Al_2O_3 ceramics can act as the solid phase, whereas the liquid phase is formed by selected additives, among which the most commonly in use are binders (polyethylene glycol, cellulose derivatives, polyvinyl alcohol), plasticizers (glycols, polyethylene oxide) or dispersants (polyelectrolytes, sodium carbonate, sodium silicate stearates)[1]. Most of the time, the binder represents the main part of the additives in the formulation of the ceramic paste. According to Blackburn *et al.*[19], extrusion is indeed only possible if the binder surrounds each of the particles of the ceramic powder. Then the plasticizer modifies the binder, increasing the flexibility of the formulation, thus facilitating the stacking and cutting of the pieces[8]. For example, Zhang *et al*.[20] found that glycerol softened the ceramic paste, thus improving the edge definition of the printed pieces. Considering that, most binders and plasticizers are organic and must therefore be removed during a debinding step before the densification and sintering of the sample, the use of a large amount of additives inevitably leads to longer debinding steps, increasing the probability of defects in the extruded pieces[21]. To avoid such defects, a rise in the solid load of the paste results in the reduction of its organic matter content and a better-expected quality of the ceramic pieces after sintering[16]. Tang *et al.*[21], prepared highly loaded slurries of Al_2O_3 using acetic acid as a dispersant, a methylcellulose solution as a binder, and extruded the resulting aqueous ceramic paste using a 3D printer. The formulations initially presented a shear-thinning (viscoelastic) rheological behavior. However, while varying the Al_2O_3 load proportions (from 46 to 52 vol%), they observed a collapsing phenomenon and a poor shape retention related to the low solid load of the slurry. In fact, when the Al_2O_3 proportion in the slurry was at least 50 vol%, the extruded filaments displayed a uniform morphology without deformation and a smoother surface. Jinsong *et al.*[16], also found out that an optimal Al_2O_3 proportion of 50 vol% in the slurries containing glycerol as a lubricant,

ammonium citrate as a dispersant and poly vinyl alcohol as a binder, resulted in an improvement of the surface quality. Carloni *et al.*[22], increased the Al_2O_3 (with 0.063 wt% MgO) solid load to 72 wt% and added ISOBAM 104 as a binder and dispersant (0.7 wt%) to prepare a printable slurry able to shape transparent ceramics after post-processing steps. Furthermore, they found out that a slight increase in the ISOBAM 104 resulted in a viscosity increase of an order of magnitude. Thus, it seems that setting a high solid load and changing the additives' proportions could be another path to extrude a filament that will be able to resist deformation and shrinking after printing, leading to a consolidated ceramic. Several authors in the literature have found that sintered parts manufactured by additive manufacturing have a different % shrinkage in the Z-axis compared to the X and Y axes. Su *et al.*[23], found that alumina pieces treated thermally at 1550 °C had a % shrinkage increment in the X-axis of 12 and in the Y-axis, 15 %. However, in the Z-axis, the % shrinkage increased to 21.4 %. These authors attributed this difference of % shrinkage in the Z-axis to the "friction free" of the pieces during sintering. They said there was no Z-axis constraint that hindered sintering shrinkage as opposed to the X and Y-axis, where the frictional constraint may result in a mechanical interlocking, reducing the shrinkage in that plane[23]. Likewise, Tsui and collaborators[24], found that alumina samples after being treated at 1625 °C, had a different % shrinkage in Z-axis, while in the X and Y axes, % shrinkage was similar. They attributed this greater % shrinkage to the elimination of a higher void density during sintering in the Z-axis.

The aim of this work was thus to prepare Al_2O_3-based pastes that can be extruded, while presenting a high ceramic load (>75 wt%), as well as to assess their maximum supported load. In first instance, this investigation of alumina pastes will support the development of refractory pastes of ceramic materials with greater resistance to creep at high temperatures, such as yttrium aluminum garnet, YAG. Since the synthesis of a large amount of YAG is necessary to make complete studies, the use of alumina instead of YAG in the early investigations will reduce,

principally, the cost of raw materials. A practical evaluation of the alumina pastes extrudability was made with each increment of the charge. The additives used in the pastes were polyvinyl alcohol, glycerol and ISOBAM 104. Thermal and structural properties of the pastes and sintered samples before and after thermal treatments were analyzed.

2. EXPERIMENTAL PROCEDURE

2.1 Preparation of the pastes

Commercial alumina powder (Ceradel, mean grain size 8.3 µm and $\rho = 3.97$ g/cm^3) was used as a solid load to formulate the ceramic pastes, then, glycerol (99%, extra pure, ACROS Organics) was added as a plasticizer without further treatment. Finally, two aqueous solutions were prepared, namely polyvinyl alcohol, PVA, (Rhodoviol 25/140, VWR Chemicals), as a binder and ISOBAM 104 (Kuraray Co., Ltd, Osaka, Japan) as a binder and dispersant. Preparing the latter required 6 g of ISOBAM 104 and 120 cm^3 of distilled water, mixed overnight under stirring, whereas a similar protocol was followed with specific quantities of PVA to prepare the PVA aqueous solution.

Ten paste formulations were studied with the aim of determining a link between composition and printability. For each of them, alumina powder (> 75 wt%) was mechanically mixed while adding different specific quantities of PVA (< 2.15 wt%), glycerol (< 2.56 wt%) and ISOBAM 104 (< 0.03 wt%). All the resulting mixtures were prepared under stirring at 240 rpm/20 min at 25 °C. **Fig. 1** shows the general protocol implemented for the preparation and the extrusion of the pastes, whereas their compositions are reported in **Table 1**.

2.2 Extrusion of the pastes and consolidation of the pieces

The pastes were extruded with a commercial 3D ceramic printer (Delta WASP 2040 clay) displaying printing volume dimensions of Ø 200 mm x h 400 mm and a liquid deposit modeling extruder with a 2 mm diameter nozzle. Once the paste was prepared and placed inside the printer tank, the ceramic paste was extruded under the following experimental conditions:

a 4 bars compressed air flow, a 2 mm/s printing speed, 1.5 mm high layers and a temperature of 20 °C with 50 % of relative humidity (RH). Finally, the .stl file (3D model of the piece) was edited and sliced using the CURA software in order to obtain the g-code program required by the printer. Several pieces were then printed with each alumina paste to confirm their stability. After extrusion, the green samples were dried at room temperature during 18 h in air with 50 % RH, and were then heated in a furnace (Ceradel CT15) during 3 h at 650 °C with a 1 °C/min heating rate under static air, in order to eliminate the organic content. The ceramic consolidation was carried out in a tubular furnace (Carbolite STF 16/180) during 3 h at 1400 °C with a 2 °C/min heating rate under a dynamic airflow of 0.2 L / min, as shown in **Fig. 2**.

2.3 Characterization

Each fresh alumina paste was loaded in a syringe and, by weighing its mass contained in a given volume, its density was calculated. Concerning dried samples at room temperature and calcined pastes, their relative density was measured with a helium pycnometer (AccuPycII 1340, Micromeritics). A sample was placed inside a 1 cm^3 chamber before Helium gas was admitted and then expanded into another precision internal volume. Both pressures, before and after expansion, were registered and used to measure the sample's volume. This operation was repeated 10 times.

Thermogravimetric analyses (TGA) were conducted with a SDT Q600, TA Instruments. The measurements were performed in a platinum crucible under a 100 mL/min dry airflow. The samples were heated at 1200 °C with a 5 °C/min heating rate under air. In order to analyze the thermal behavior of the pastes and the decomposition of their additives, a synchronous thermal analyzer coupled with quadrupole mass spectrometry (STA QMS 449 F3A-1398-M, NETZSCH) was used between room temperature and 600 °C with a 5 °C/min heating rate under an argon atmosphere. The QMS measurements were performed in a scanning mode for mass-to-charge ratio (m/z) in the range of 1 to 100 amu.

The microstructure of the samples were then observed using a scanning electron microscope (FEI quanta 450 FEG, Thermo Fisher Scientific, Eindhoven), using a low field detector with a 5 kV beam voltage and a 10^{-5} Pa chamber pressure. In the case of the pastes without thermal treatment, the extruded pieces were dried at room temperature during 72 h prior to the measurements before they were cut off and placed inside the sample holder. No further treatment was applied.

The shrinkage percentage, % shrinkage, was measured after heat treatments on printed parallelepipeds of 2.5 x 2.5 x 4.5 mm side made with the same alumina paste as the samples. The measures were carried out with a digimatic caliper (Mitutoyo, Model CD-P15P, Japan). The % shrinkage was calculated for comparison according to the Eq. 1:

$$\%\ shrinkage = \frac{L_1 - L_2}{L_2} * 100\% \quad (1)$$

Where L_1, is the initial length in mm of the specimen before the thermal treatments and the L_2, is the final length in mm of the specimen after thermal treatments. The % shrinkage was calculated in X, Z and Y axes.

3. RESULTS

3.1 Printability of very highly loaded alumina pastes

Detailed formulations of the pastes and their corresponding measured densities are listed in **Table 1**. Moreover, **Fig. SF1,** in the supplementary file, shows different printed pieces, dried at room temperature during 18 h in air with 50 % RH. Whatever their design, which depends on the original .stl file, the printing quality of the samples, and thus the printability of the pastes, can be evaluated by studying those extruded pieces. Hence, several criteria, based on a careful visual examination of the samples, were selected in order to determine their quality; this included the general definition of the shapes and their corner finishing, the continuity of the printing and the extruded filament morphology.

Firstly, in pastes #1 to #3, the solid load remained constant (79.87 wt%), while the PVA and glycerol proportions were modified. As the amount of glycerol increased from 0.96 to 2.56 wt%, the extruded filament became smoother and with a more homogeneous shape, and the continuity of the printing was improved as well. A combination of small amounts of glycerol compensated by greater amounts of PVA led to an unfilled printed piece with a dry aspect, as it can be observed in paste #1. Paste #2, containing 1.6 wt% of glycerol, showed better-defined corners and overall shape than its neighbors, but its very high load of alumina caused an occasional clogging of the nozzle. However, using even greater amounts of glycerol (2.56 wt%) resulted in a mechanically weak initial layer unable to sustain additional layers on top of it, as illustrated with paste #3. A proportion of glycerol close to 1.6 wt% was thus further used in order to favor printing and to ensure well-defined corners and shapes for the extruded pieces[20]. Based on those previous observations, paste #4 was therefore prepared with a slightly lower amount of solid load (79.37 wt%) and adjusted quantities of additives. As a result, the extruded piece was completely filled with a continuous filament and its corner and shape were very well defined, while the obstruction of the nozzle issue was solved.

Secondly, based on the last formulation, pastes #5, #6 and #7 were prepared with the gradual addition of ISOBAM 104 as a second binder. Besides, as the PVA and the ISOBAM 104 were dissolved in water, the water content increased with the addition of ISOBAM 104. However, concerning these three pastes, the content of water remained at about 17.60 wt%, as the extra quantity of additive is low. Paste #5, prepared with the least ISOBAM 104, displayed a very similar printability to paste #4. This was expected, as their formulations are very close, including the water content. Paste #6 was also printed with a continuous filament and satisfyingly defined corners, but with no clear improvement of the overall quality. However, significantly increasing the quantity of ISOBAM 104 led to a very fluid paste and a soft and poorly defined piece, as can be seen for paste #7. It is to be noted that this was not the case for

Carloni and collaborators[22], where a higher addition of ISOBAM 104 (0.7 wt%) and the use of other additives (such as MgO) lead to the preparation of an extrudable high solid loaded paste around 72 wt%.

Finally, higher amounts of PVA were introduced in pastes #8 and #9, coupled with a smaller proportion of solid load, in order to assess the effect of this PVA quantity. Although the glycerol proportion was kept at around 1.6 wt%, these printed pieces were not well defined, as the pastes were very fluid, resulting in poor printability. An additional experiment was carried out for paste #10, as it was prepared using exclusively aqueous PVA mixed with alumina. As expected, the printed piece displayed a low resolution at its edges.

In conclusion, in the case of a high load of alumina, it exists suitable proportions of additives that can lead to an extrudable paste able to shape defined printed pieces with an interlayered structure. In our case, the pastes #4, #5 and #6 performed the best. However, pastes #5 and #6, containing ISOBAM 104, they got very dry **after** extrusion, making difficult the manipulation of the printed samples. For this reason, hereinafter, paste #4 will be considered like the best paste presenting good printability.

Fig. 3 (a) displays the concentration of aluminum, [Al], in each paste; the pastes presenting a higher [Al] contained a major solid load of alumina and consequently a lower proportion of additives. Based on Fig. 3(a) it is then possible to divide the pastes into three families: pastes #1, #2 and #3 form family I, pastes #4, #5, #6 and #7, family II and pastes #8, #9 and #10 are gathered in family III. Family I represents the pastes with the highest solid load among the ten samples (79.87 wt%), with an [Al] varying from $1.25x10^{-2}$ to $1.29x10^{-2}$ $mol.L^{-1}$. These pastes were characterized by a poor printability and a problematic extrusion. Regarding family II, the quality of the pastes and printing has improved significantly, with an [Al] decreasing down to $1.06x10^{-2}$ $mol.L^{-1}$. Family III gathers very fluid pastes with an [Al] lower than $1.0x10^{-2}$ $mol.L^{-1}$, giving rise to low-quality printed parts. It thus seems that an [Al] of about

$1.08x10^{-2}$ $mol.L^{-1}$ is suitable in order to ensure good printability, as seen for pastes #4, #5 and #6 (family II), among which paste #4 had the highest solid load (79.37 wt%). Note that the absence of paste #7 between the best candidates for extrusion, suggests that paste #7 is in transition between family II and III.

Concerning the density of the fresh pastes, additives were present in greater proportion as the alumina load was reduced. This results in a decrease in the density of the paste, as shown in **Table 1**. To illustrate this point, **Fig. 3 (b)** displays the density of the fresh pastes as a function of the Al_2O_3 to water molar ratio $\frac{\text{n } Al_2O_3}{\text{n water}}$. Different tendencies were identified, dividing once more the samples into three families. The first tendency involved family I, with samples characterized by a molar ratio between 0.8-0.9 and a high density, since they contain a high solid load of alumina (79.87 wt%). For this family, $\frac{\text{n } Al_2O_3}{\text{n water}}$ slightly increased as the quantity of PVA decreased, as being water-based. For the second tendency observed, the molar ratio and densities values remained close while the proportions of glycerol and PVA were constant (pastes #4, #5, #6 and #7 from family II). However, as the ISOBAM 104 (also water-based) was added in the paste formulations, the molar ratio $\frac{\text{n } Al_2O_3}{\text{n water}}$ decreased. Finally, when the PVA proportions were raised, a clear drop of $\frac{\text{n } Al_2O_3}{\text{n water}}$ was observed in pastes #8, #9 and #10, their densities remaining relatively stable. Paste #10, prepared exclusively with PVA, presented the lowest $\frac{\text{n } Al_2O_3}{\text{n water}}$ and density of the lot. In conclusion, the density of fresh pastes was not only related to their solid load or their water content, as it seems that good printability required respecting a specific range of properties, outside of which the quality of the samples is difficult to maintain.

Again, some special attention should be paid to pastes #4, #5 and #6 (family II). They indeed exhibit very similar characteristics and present the best printability performance with a high solid load (> 79 wt%).

Another perspective of the factors affecting the extrudability of pastes, in addition to the [Al] and $\frac{\text{n } Al_2O_3}{\text{n water}}$ ratio parameters, is the elucidation of the interface between the developed surface of the Al_2O_3 particles and the liquid phase of the pastes. **Fig. 4 (a),** displays the binder molecules per developed surface of the Al_2O_3, $\frac{molecules}{nm^2}$, and the reverse of the estimated volume of the liquid phase for the 10 pastes. Like in the plots of [Al] and $\frac{\text{n } Al_2O_3}{\text{n water}}$ ratio, here it was possible to observe three trends that coincided with the family I, II and III. As the number of binder molecules reported to the developed surface of the solid load were almost constant in the three mentioned families, we can reasonably consider that most of the particles were nicely covered whatever the formulation of the paste. The extrudability of the paste seemed then mainly related to the network of residual intertwined binder molecules in water. The reverse of the estimated volume of the liquid phase for the paste series simply compared the concentration of residual binder molecules in the liquid phase. This indicator was proportional to the concentration of residual binder in the liquid phase, and could help to schematize the situation for pastes #3, #4 and #9. For the paste #3, we can figure a scheme related to Fig. 4 (b), where the concentration of binders was definitively too high and leads to a high degree of intertwined binder molecules in the liquid phase, which degraded the extrudability of the paste. Concerning paste #4 issued from family II, which was the best extrudable family in this study, we can suppose that the all the components namely relative contents of solid load, binder and water were perfectly fitted and resulted in good extrudability, see **Fig. 4. (c)**. In contrast, for paste #9 from family III, represented by the scheme **Fig. 4 (d)**, the poor concentration of additives would form a fluid paste, unable to be extruded.

These schematic representations of the interface between the developed surface of the Al_2O_3 particles and the liquid phase of the pastes, agree with the extrudability results relating the [Al] and $\frac{\text{n } Al_2O_3}{\text{n water}}$ ratio parameters, where the best printability belonged to pastes #4, #5 and #6. It is

important to note that, although paste #1 is close to those of pastes #4, #5 and #6, the glycerol proportion in paste #1 was too weak (0.96 wt%) and thus reduced the quality in printing.

3.2 Temperature behavior of the alumina pastes

A few pastes displaying different behaviors during printing has been selected at the rate of one per previously specified families: pastes #3, #4 and #9, see **Fig. 5**. Their thermal behavior was then studied in order to determine if it is possible to identify specific characteristics in the formulations that are best suited for extrusion.

The thermal curves of these samples are gathered in **Fig. 6**. With an endothermic phenomenon at around 70 °C and exothermic peaks associated to weight losses between 150 and 600 °C, all thermograms presented similar characteristics. After 600°C, the different masses of the samples remained stable, confirming the choice of the debinding temperature. **Fig. (6a)** shows the first analyzed sample, paste #3, which exhibited a weight loss of 15% at 120 °C related to water elimination[25]. The other three weight losses observed at 230, 370 and 450 °C were connected to exothermic reactions[26,27], and corresponded to a global weight loss of 4 % resulting from decomposition of organics. Similar behavior was observed for paste #9 at 120, 250 and 475 °C, with weight losses of 19, 4, 1% respectively. These temperatures had higher values of weight losses involved, which is logical considering their lower solid load. However, despite a first endothermic peak and the mass loss it represented, as well as the rest of the thermal analysis being generally comparable to the other samples, it appears that paste #4 exhibited a barely identifiable exothermic peak at 430 °C corresponding to the second weight loss of 0.5%.

In order to study the different phenomena that occurred during the elimination of the organic residues and solvent, mass spectra analyses of pastes #3, #4 and #9 were performed during their thermal treatment. Although the complete results can be consulted in the supplementary file (**Fig. SF2, SF3 and SF4**), the departures' monitoring of the elements corresponding to the m/z 18, 29 and 44 were selected due to their greatest intensities in the mass spectra measurements,

as seen in **Fig. 7**. Three distinct zones can be identified, in agreement with the mass losses observed by TGA: the first one from 20 to 100 °C, the second from 150 to 350 °C and the third for temperatures above 350 °C. In the first zone, the m/z = 18 contribution showed a well-defined and intense contribution for all the three pastes. These peaks can be associated to water elimination and water formation during the decomposition of the PVA and glycerol additives contained into the paste. This phenomenon is particularly well defined for paste #3, which contained the highest quantity of water in its formulation. In the second zone (150 to 350 °C), the three selected m/z values presented an intense contribution centered around 250 °C, which can be related to the PVA ($(-CH_2CHOH-)_n$) degradation into hydrocarbons like CH_3-CH_2 (m/z 29) and water and to the formation of CO_2. Besides, the decomposition of pure glycerol in air occurred in a single step in this temperature[28] range. In the third zone (T > 350 °C), m/z 44 displayed a low intensity contribution for some samples, which can be related to the last weight loss observed by TGA, and might be assigned to the oxidation of carbon residues into CO_2. This could then indicate that in some cases the decomposition occurring in the second zone is incomplete, leading to carbon residues upon heating due to a possible lack of oxidizing agents as the thermal analysis was conducted in an inert argon atmosphere. This was especially noticeable for the paste #9, which had the highest amount of additives and the highest $\frac{PVA}{glycerol}$ ratio (1.17), compared to pastes #3 and #4's respective ratios of 0.61 and 1.06. This tends to confirm the final PVA chains decomposition[29] as a possible source for this last phenomenon. Besides, the difficulty to visualize this contribution for pastes #3 and #4, although containing the same additives, could then be explained by the efficiency of the degradation of the additives mixture, which is improved as more glycerol is present in the formulation. The decomposition products of glycerol can indeed have a cooperative effect on the oxidation of the PVA, promoting the departure of organics. Then, paste #4 displayed an interesting phenomenon for each m/z, as its thermal contributions were observed at slightly higher temperatures than for the

other pastes, especially in the second zone (150 °C to 350 °C), without detecting a signature for the weight loss occurring between 400 and 500 °C. Such a delay could be explained by a modified decomposition sequence or a different cooperative decomposition between the two kinds of additives, as they were mixed in relatively close amounts. In conclusion, paste #4 showed that an optimal decomposition of additives takes place at once, although at slightly higher temperatures, resulting in an overall more effective elimination of organics.

The evolution of the microstructures was observed by SEM, in order to estimate their original compactness and identify whether the debinding step might alter the samples. **Fig. 8** presents the micrographs of the printed samples prepared with pastes #3, #4 and #9, either after drying at 25 °C or after calcination at 1400 °C. The cross-sectioned pieces of pastes #3 and #9 revealed a grainy aspect and randomly stacked particles or agglomerates. On the other hand, the sample printed from paste #4 presented a homogeneous microstructure with well-aligned grains. This indicates that the composition and amounts of the additives used in the formulation greatly diminished the friction of the grains during the extrusion process, leading to a relatively smooth fracture surface. After calcination at 1400 °C, the morphologies of the three samples remained very similar to their room temperature counterparts. It seems that the debinding step and the removal of the organics did not create any major fracture or decohesion of the pieces, with no increase in the grain sizes observed at this temperature. However, the sample printed from paste #4 still presented a much smoother fracture surface than the other two, which confirms that the easier printing observed with this paste is also related to a more homogeneous microstructure in terms of size and shape. It seems that the organics' decompositions occurring in this paste were sufficiently controlled to limit the formation of major open porosity in the sample. Furthermore, the density of the samples treated at 1400 °C was measured in order to validate the complete elimination of additives. Regardless of the sample, the measured density

after calcination is close to the alumina's (3.97 g/cm^3)[30], confirming first that the samples are free of organics, and second that no closed porosity can be evidenced.

An extruded sample of paste #4 was heated at 1700 °C in order to study its thermal behavior at a higher temperature, as the sintering temperature of alumina is known to be normally higher than 1500 °C. **Fig. 9 (a)** shows the alumina piece after thermal treatment and **Fig. 9 (b)** its fracture surface's microstructure observed by SEM. As compared to the micrographs of the same sample heat-treated at 1400 °C, an obvious grain growth effect remaining controlled can be observed, and the sintering occurred with no major stacking modification of the grains.

3.3 Shrinkage after thermal treatments

The % shrinkage of paste #4 heated at 1700 °C was measured in the three dimensions, see **Fig. 10**. The % shrinkage in X-axe increased from 0.3 at 650 °C to 8 at 1700 °C; the shrinkage of Y-axe increased to 2 at 650 °c to 6.8 at 1700 °C; the shrinkage in Z-axe increased to 4.8 at 650 °C and then increased to 13.8 at 1700 °C. These measurements showed that shrinking in X and Y-axes after debinding and calcination is very similar. Despite this, in Z-axe the shrinking was more evident. This can be explained due to the fabrication of the piece and the sintering mechanisms during thermal treatments. The pieces were fabricated by additive manufacturing; this implied that between each layer, the generation of imperfections and voids was more probable. When building the piece, the X-Y plane was not affected by external factors of additive manufacturing as the paste filament was deposed in the same plane (X, Y). However, in Z direction, the stacking of the layers caused these voids to accumulate, modifying the packing of the border grains. These imperfections became more evident after thermal treatments. During sintering, the alumina grains grew, making the microstructure more closed and dense, leading to the elimination of voids. This greater shrinkage in the Z-axis was already reported in the literature by distinct authors[31, 32, 33]. A comparison between this work

and those in the literature with similar conditions can be seen in **Fig. 11**. As the alumina pieces consolidated, % shrinkage in the Z-axis increased. At 650 °C, temperature below alumina sintering, the % shrinkage was about 4.8 %. When the diffusion mechanisms began, around 1200 °C, the % shrinkage decreased between 0.5 and 1. As the temperature increased, between 1500-1700 °C, the microstructure of the alumina pieces densified. This greatly increased the % shrinkage at Z; for Su *et al.*[23], at 1550 °C, the shrinking in Z-axis was around 21.4 % and for Tsui *et al.*[24], at 1625 °C, it was about 23%. However, compared with the others sintered samples from bibliography, the alumina sample prepared in this investigation (paste #4), reached the lowest shrinkage value (13.8%) at 1700 °C.

4. CONCLUSIONS

High-loaded alumina pastes (solid load > 75 wt%) were prepared using glycerol and an aqueous solution of PVA and ISOBAM 104 as additives. Several parameters influenced the extrudability of the paste; for example, the organic additives-to-aluminum molar ratio was a key factor to obtain good quality samples. In this study, pastes formulations containing 75< Al_2O_3 < 80 wt% (63.5 vol%), 1.56 (17.77 vol%) < PVA < 2.15 wt% (25.84 vol%), glycerol < 2.56 wt% (1.65 vol%) and ISOBAM 104 < 0.03 wt% (0.63 vol%) were investigated. The printability of the pastes was then evaluated as a function of the organic additives to aluminum molar ratio. The best printability was witnessed where the Al_2O_3 charge was around 79 wt%. The ISOBAM 104 did not seem to have a major beneficial influence when it was added to the PVA and glycerol additives. According to SEM analysis, the most homogeneous microstructure was achieved when the extruded sample from paste #4 was sintered at 1700 °C. At this temperature, a shrinkage of 13.8 % in the Z-axis was reached, being one of the lowest shrinkage values found in the literature. Thanks to this preliminary investigation of extrudability of high loaded alumina pastes, would be possible to pursue a similar research, now with creep-resistant

ceramics, like yttrium aluminum garnet, YAG. Those pieces would be produced by additive manufacturing, from high loaded pastes, to print stator/rotor turbine parts.

5. REFERENCES

[1] Soboyejo W.O., Obayemi J.D., Annan E., Ampaw E.K., Daniels L., Rahbar N., Review of high temperature ceramics for aerospace applications. Adv. Mater. Res. 1132, 385–407 (2016). https://doi.org/10.4028/www.scientific.net/AMR.1132.385

[2] A.S. Koroteev, D.I. Andrianov, A.V. Karevskiy, E.N. Kiryushin, A.V. Popov, A.V. Semenkin, A.E. Solodukhin, L.E. Zakharenkov, F. Jansen, T. Brandt, V. Maiwald, W. Bauer, A.M. Gomez, S.S. Jahnke, M. Hillebrandt, M. Richter, S. Ferraris, M.C. Tosi, F. Masson, J. Combettes, S. Oriol, J.-C. Worms, E. Detsis, M. Muszynski, F. Lassoudière, R. Granjon, T. Tinsley, Z. Hodgson, J.A.P. Findlay, L.N.F. Guimarães. 2017. Test Bench for Key Components of Megawatt Class International Power and Propulsion System Ground Demonstration. Conference: 7th European Conference for Aeronautics and Space Sciences (EUCASS). Milan, Italy. (2017) DOI: 10.13009/EUCASS2017-198

[3]Bhowmik, R.N., Ranganathan, R. Existence of two spin dynamics in the temperature and magnetic field dependence of the magnetization curves of ferrimagnetic Co1.75Fe1.25O4 and its composite with BaTiO3. J. Phys. Chem. Solids 155 (2021). https://doi.org/10.1016/j.jpcs.2021.110103

[4]Guo, X., Gin, S., Frankel, G.S. Review of corrosion interactions between different materials relevant to disposal of high-level nuclear waste. Npj Mater. Degrad. 4:34 (2020). https://doi.org/10.1038/s41529-020-00140-7

[5]Gao, X., Cheng, Z., Chen, Z., Liu, Y., Meng, X., Zhang, X., Wang, J., Guo, Q., Li, B., Sun, H., Gu, Q., Hao, H., Shen, Q., Wu, J., Liao, X., Ringer, S.P., Liu, H., Zhang, L., Chen, W., Li, F., Zhang, S. The mechanism for the enhanced piezoelectricity in multi-elements doped (K,Na)NbO3 ceramics. Nat. Commun. 12:881 (2021). https://doi.org/10.1038/s41467-021-21202-7

[6]Feng, C., Zhang, K., He, R., Ding, G., Xia, M., Jin, X., Xie, C. Additive manufacturing of hydroxyapatite bioceramic scaffolds: Dispersion, digital light processing, sintering, mechanical properties, and biocompatibility. J. Adv. Ceram. 9 (3), 360–373, (2020). https://doi.org/10.1007/s40145-020-0375-8

[7]Yashima, M., Tsujiguchi, T., Sakuda, Y., Yasui, Y., Zhou, Y., Fujii, K., Torii, S., Kamiyama, T., Skinner, S.J. High oxide-ion conductivity through the interstitial oxygen site in Ba7Nb4MoO20-based hexagonal perovskite related oxides. Nat. Commun. 12:1, (2021). https://doi.org/10.1038/s41467-020-20859-w

[8]Chartier T., Ceramic Forming Processes, in: Boch, P., Nièpce, JC. (Eds.). Ceramic materials: processes, properties and applications. ISTE Ltd., London. 2007 pp. 123-194

[9] Curto H., Thuault A., Jean F., Violier M., Dupont V., Hornez J.-C., Leriche A. Coupling additive manufacturing and microwave sintering: a fast processing route of alumina ceramics. J. Eur. Ceram. Soc. (2019), p. 1, 10.1016/j.jeurceramsoc.2019.11.009

[10] Chugunov, S., Adams, N.A., Akhatov, I. Evolution of SLA-Based Al2O3 microstructure during additive manufacturing process. Materials 2020, 13, 3928. https://doi.org/10.3390/MA1318392

[11] Mariani, M., Beltrami, R., Brusa, P., Galassi, C., Ardito, R., Lecis, N. 3D printing of fine alumina powders by binder jetting. J. Eur. Ceram. Soc. 41:10 (2021), 5307–5315. https://doi.org/10.1016/j.jeurceramsoc.2021.04.006

[12] Ziaee M., Crane N.B. Binder jetting: a review of process, materials, and methods. Additive Manufact., 28 (2019), pp. 781-801, 10.1016/j.addma.2019.05.031
[13]Dermeik, B., Travitzky, N. Laminated Object Manufacturing of Ceramic-Based Materials. Adv. Eng. Mater. 22 (2020), Article 2000256. https://doi.org/10.1002/adem.202000256
[14] Wu, J.-M., Li, M., Liu, S.-S., Shi, Y.-S., Li, C.-H., Wang, W. Selective laser sintering of porous Al2O3-based ceramics using both Al2O3 and SiO2 poly-hollow microspheres as raw materials. Ceram. Int. 47:11 (2021), 15313–15318. https://doi.org/10.1016/j.ceramint.2021.02.096
[15]Shahzad, K., Deckers, J., Zhang, Z., Kruth, J.-P., Vleugels, J. Additive manufacturing of zirconia parts by indirect selective laser sintering. J. Eur. Ceram. Soc. 34:1 (2014), 81–89. https://doi.org/10.1016/j.jeurceramsoc.2013.07.023
[16]Jinsong, C., Enquan, B., Dazhi, H., Yunfei, D., Xuhui, Q. Extrusion Freeforming-Based 3D Printing of Ceramic Materials. Mater. Trans. 61:11, 2236–2240 (2020). https://doi.org/10.2320/matertrans.MT-M2020167
[17]Peng, E., Wei, X., Herng, T.S., Garbe, U., Yu, D., Ding, J. Ferrite-based soft and hard magnetic structures by extrusion free forming. RSC Adv. 7:43, 27128–27138 (2017). https://doi.org/10.1039/c7ra03251j
[18]Li, W., Armani, A., Martin, A., Kroehler, B., Henderson, A., Huang, T., Watts, J., Hilmas, G., Leu, M. Extrusion-based additive manufacturing of functionally graded ceramics. J. Eur. Ceram. Soc. 41:3, 2049–2057 (2021). https://doi.org/10.1016/j.jeurceramsoc.2020.10.029
[19]Blackburn, S., Böhm, H. The influence of powder packing on the rheology of fibre-loaded pastes. J. Mater. Sci. 29:16, 4157–4166 (1994). https://doi.org/10.1007/BF00414194
[20]Zhang, G., Carloni, D., Wu, Y. 3D printing of transparent YAG ceramics using copolymer-assisted slurry. Ceram. Int. Part B 46:10 (2020), 17130–17134. https://doi.org/10.1016/j.ceramint.2020.03.247
[21]Tang, S., Yang, L., Li, G., Liu, X., Fan, Z. 3D printing of highly loaded slurries via layered extrusion forming: Parameters optimization and control. Addit. Manuf. 28 (2019), 546–553. https://doi.org/10.1016/j.addma.2019.05.034
[22] Carloni, D., Zhang, G., Wu, Y. Transparent alumina ceramics fabricated by 3D printing and vacuum sintering. J. Eur. Ceram. Soc. 41:1, 781–791 (2021). https://doi.org/10.1016/j.jeurceramsoc.2020.07.051
[23] Su, B., Dhara, S., Wang, L. Green ceramic machining: a top-down approach for the rapid fabrication of complex-shaped ceramics. J. Eur. Ceram. Soc., 28 (2008), pp. 2109-2115, 10.1016/j.jeurceramsoc.2008.02.023
[24]Tsui, L., Maines, E., Evans, L., David, K., and Lavin, J. M. Additive Manufacturing of Alumina Components by Extrusion of in-situ UV-cured Pastes. United States. 2018
[25] Artiaga, R., Naya, S., Garcia, A., Barbadillo, F., & García, L. Subtracting the water effect from DSC curves by using simultaneous TGA data. Thermochimica acta, 428(1-2), 137-139 (2005). https://doi.org/10.1016/j.tca.2004.11.016
[26]Yang, H., Xu, S., Jiang, L., & Dan, Y. Thermal decomposition behavior of poly (vinyl alcohol) with different hydroxyl content. Journal of Macromolecular Science, Part B, 51(3), 464-480 (2012).
[27] Dou, B., Dupont, V., Williams, P. T., Chen, H., & Ding, Y. Thermogravimetric kinetics of crude glycerol. Bioresource technology, 100(9), 2613-2620 (2019).
[28] Almazrouei, M., Elagroudy, S. & Janajreh, I. (2019). Transesterification of waste cooking oil: Quality assessment via thermogravimetric analysis. Energy Procedia. 158. 2070-2076 (2019).
[29] El-Arnaouty, M & Eid, M., Synthesis of Grafted Hydrogels as Mono-Divalent Cation Exchange for Drug Delivery. Polymer-plastics Technology and Engineering, 49. 182-190 (2010).

[30] Andersson, M., & Odén, A. A new all-ceramic crown: a dense-sintered, high-purity alumina coping with porcelain. Acta Odontologica Scandinavica, 51(1), 59-64 (1993).

[31] Gonzalez, J. A., Mireles, J., Lin, Y., and Wicker, R. B. Characterization of ceramic components fabricated using binder jetting additive manufacturing technology. Italy: 2016. doi:10.1016/j.ceramint.2016.03.079.

[32] Li, H., Liu, Y., Liu, Y., Hu, K., Lu, Z., Liang, J. Influence of Sintering Temperature on Microstructure and Mechanical Properties of Al2O3 Ceramic via 3D Stereolithography. Acta Metall. Sin. (Engl. Lett.) 33, 204–214 (2020). https://doi.org/10.1007/s40195-019-00950-y

[33] Li, H., Liu, Y., Liu, Y. et al. Effect of sintering temperature in argon atmosphere on microstructure and properties of 3D printed alumina ceramic cores. J Adv Ceram 9, 220–231 (2020). https://doi.org/10.1007/s40145-020-0362-0

Table 1. Composition and density of the alumina pastes.

Paste	Alumina		ISOBAM		PVA		Glycerol		Water		Density
#	(wt%)	(vol%)	(wt%)	(vol%)	(wt%)	(vol%)	(wt%)	(vol%)	(wt%)	(vol%)	(±0.05)
1	79.87	63.5	0	0	1.70	19.38	0.96	0.62	17.47	16.5	2.48
2	79.87	63.5	0	0	1.65	18.73	1.60	1.03	16.88	16.7	2.46
3	79.87	63.5	0	0	1.56	17.77	2.56	1.65	16.01	17.1	2.40
4	79.37	63.5	0	0	1.69	19.38	1.59	1.03	17.35	16.1	2.09
5	79.24	63.5	0.007	0.16	1.69	19.38	1.58	1.03	17.47	15.9	2.08
6	79.11	63.5	0.015	0.32	1.69	19.38	1.58	1.03	17.58	15.8	2.09
7	78.86	63.5	0.03	0.63	1.68	19.38	1.58	1.03	17.82	15.5	2.02
8	78.08	63.5	0	0	1.80	21.00	1.62	1.07	18.50	14.4	1.99
9	76.85	63.5	0	0	1.91	22.61	1.63	1.09	19.61	12.8	1.96
10	75.76	63.5	0	0	2.15	25.84	0	0	22.09	10.7	1.96

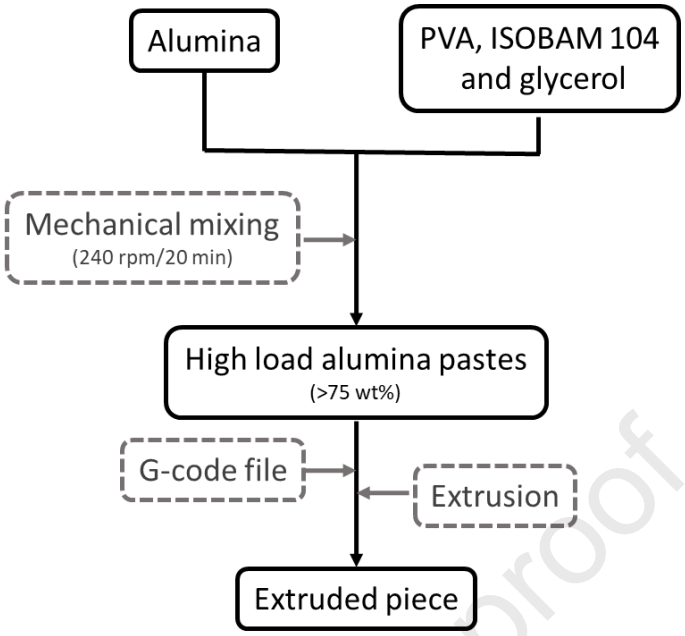

Fig. 1. Preparation protocol of the extruded alumina pieces.

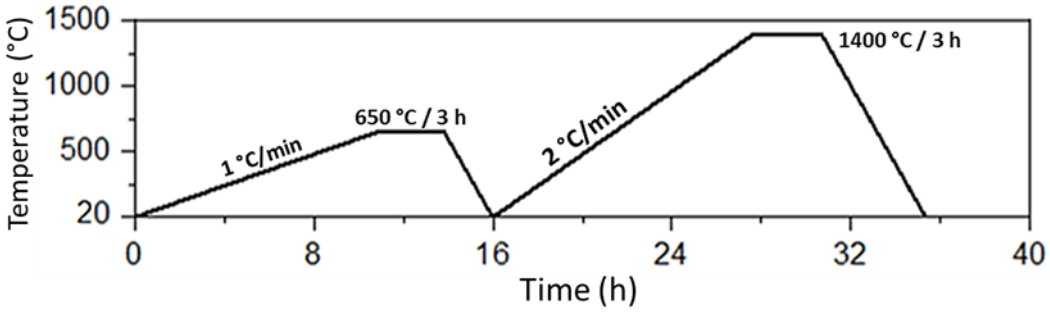

Fig. **2.** Thermal treatments of the extruded pieces made from alumina paste.

(a)

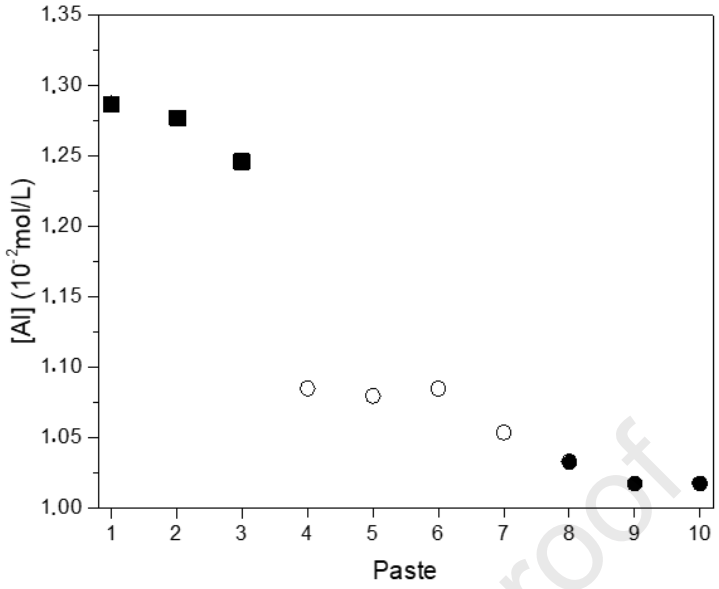

(b)

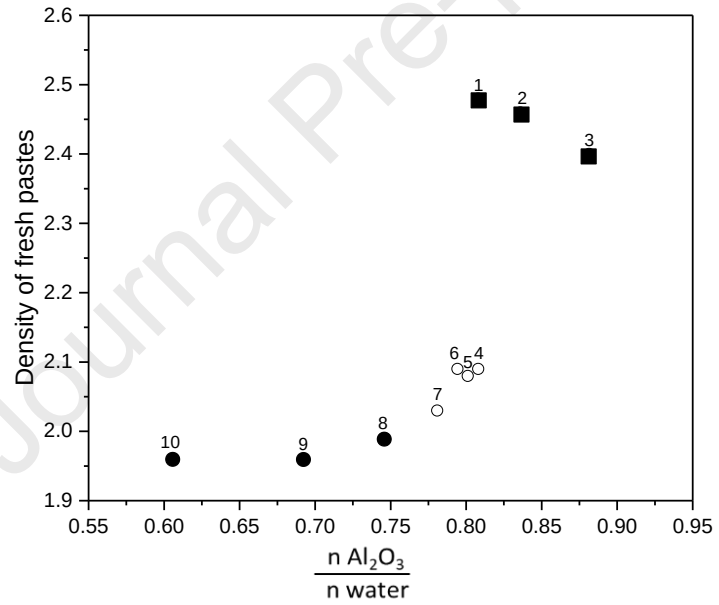

Fig. 3. (a) Aluminum concentration in the pastes and (b) density of the fresh pastes as a function of the alumina to water molar ratio with (■), (○) and (●) representing families I, II and III, respectively.

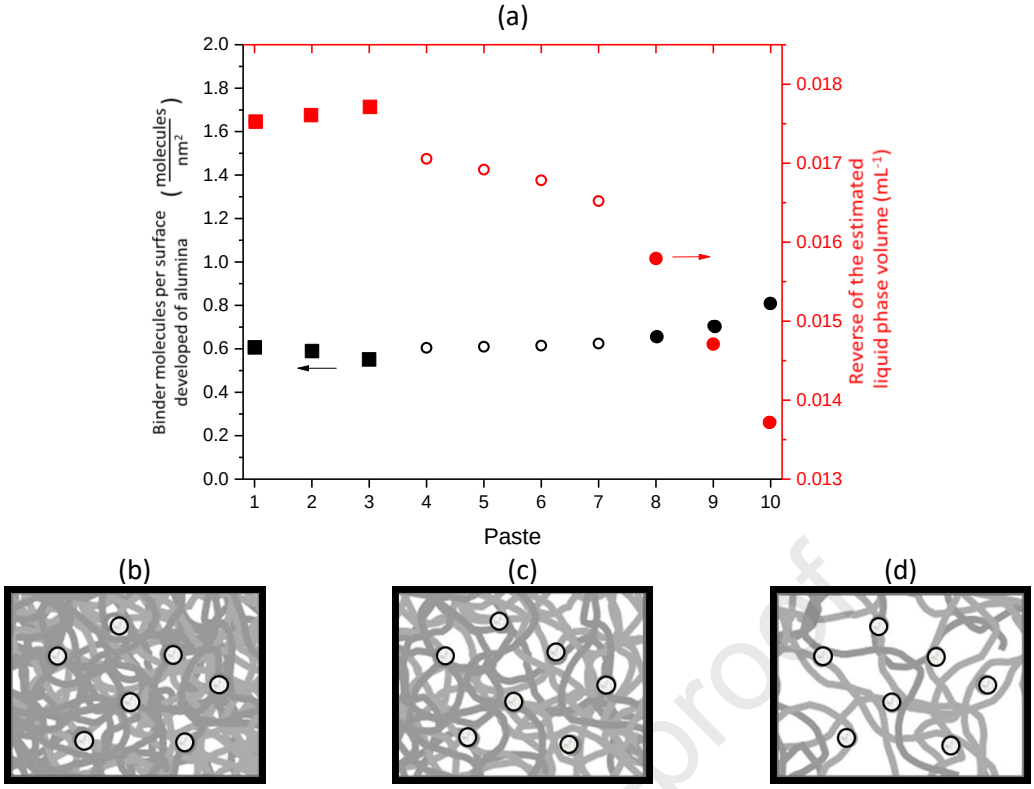

Fig. 4. (a) Estimated number of binder molecules (PVA and ISOBAM 104) and the reverse of the liquid phase volume with (■), (○) and (●) belonging to paste families I, II and III, respectively. Schematic representation of Al_2O_3 particles (spheres) and the liquid phase (intertwined network of binder molecules) for pastes (b) #3, (c) #4 and (d) #9.

Fig. 5. Raw extruded pieces of the pastes #3, #4 and #9. The formulations are in the ranges 75 < Al_2O_3 < 80 wt%, 1.56 < PVA < 2.15 wt%, glycerol < 2.56 wt% and ISOBAM 104 < 0.03 wt%. Samples 3 and 4 were intentionally broken.

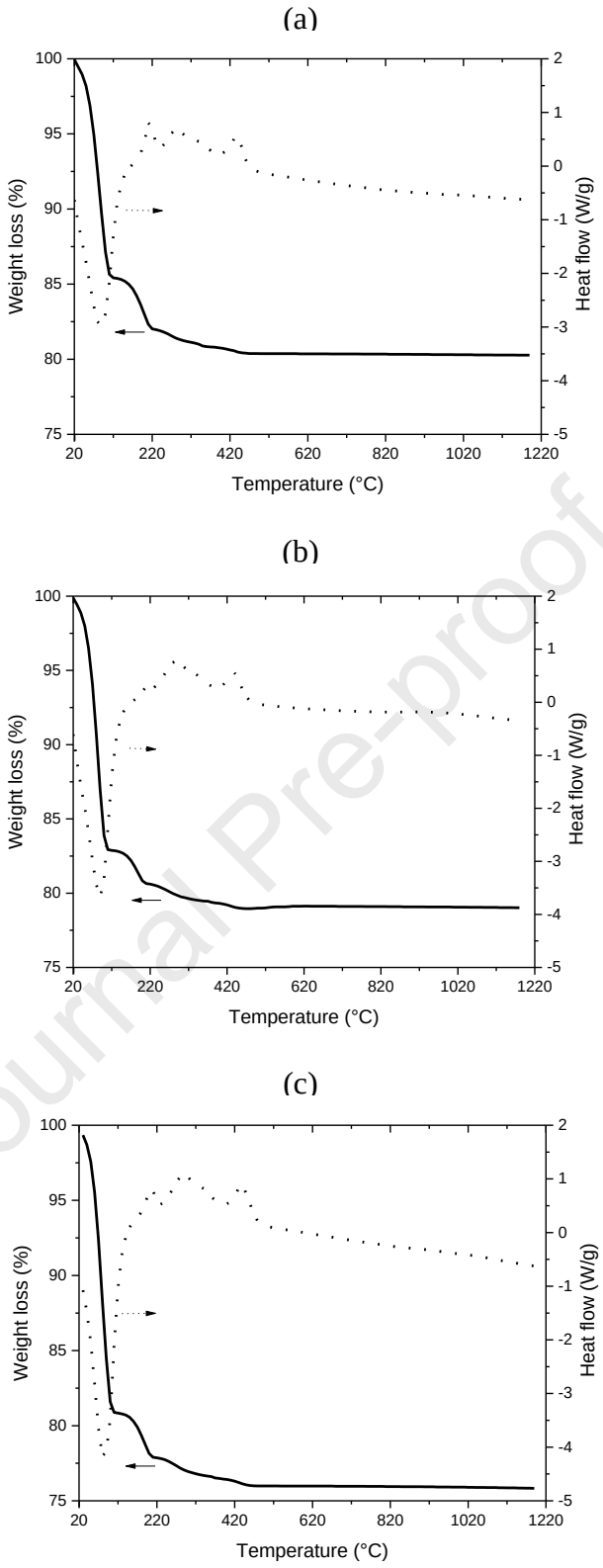

Fig. 6. Thermal curves (DTA and TGA) of (a) paste #3, (b) paste #4 and (c) paste #9.

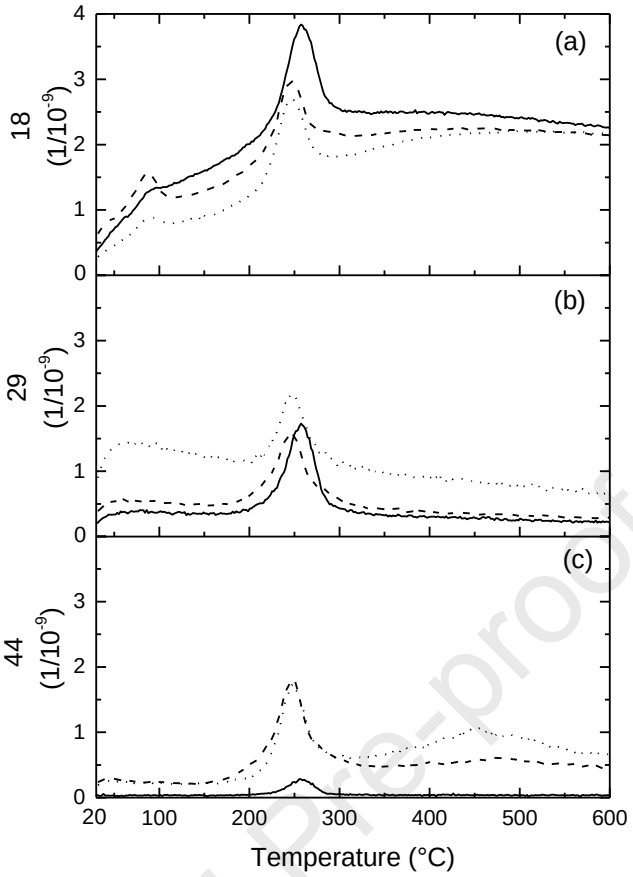

Fig. 7. Intensities of (a) m/z 18, (b) m/z 29 and (c) m/z 44 for pastes #3 (– – –), #4 (—) and #9 (···).

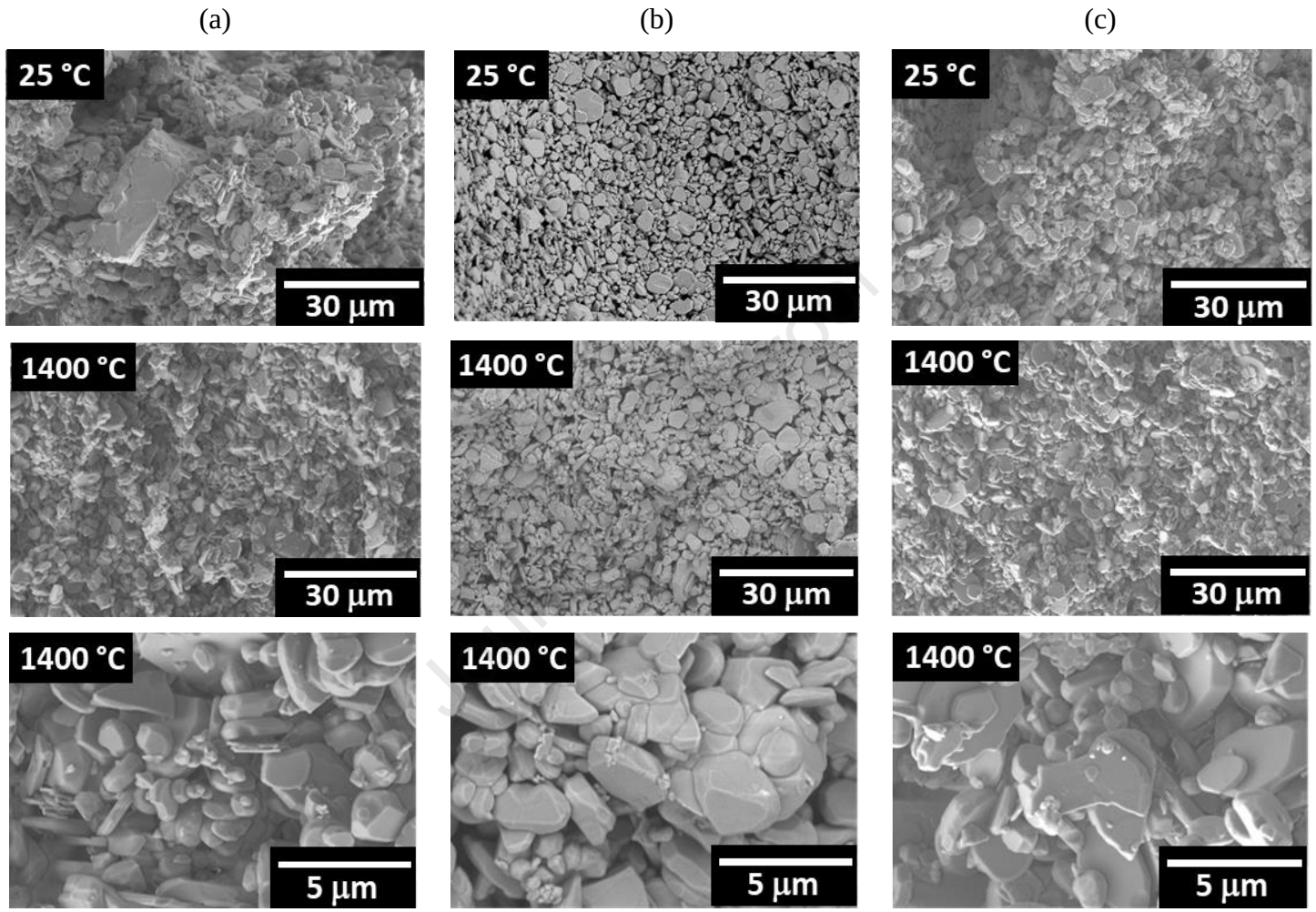

Fig. 8. SEM micrographs at 25 °C and 1400 °C of extruded samples prepared with pastes (a) #3, (b) #4 and (c) #9.

(a)

(b)

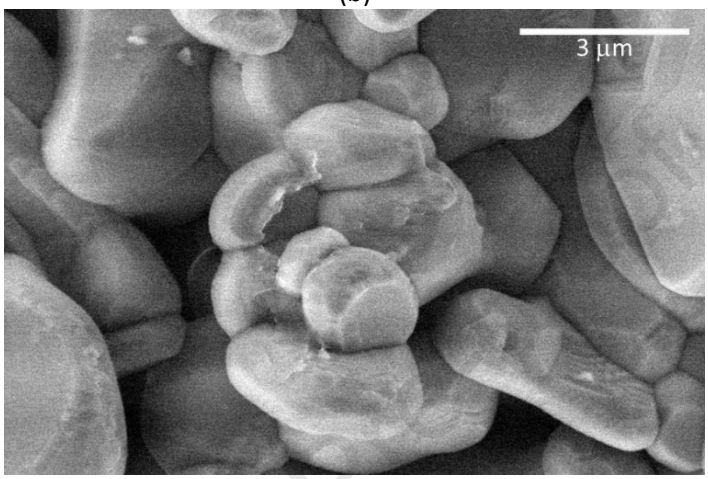

Fig. 9. (a) Extruded piece prepared with paste #4 and treated thermally at 1700 °C and (b) its SEM micrograph.

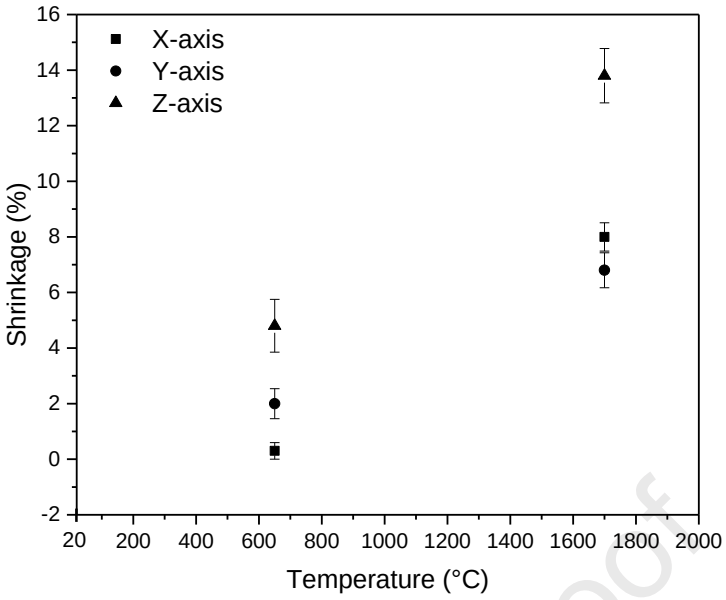

Fig. 10. Shrinkage in X, Y and Z-axes of sintered pieces prepared with paste #4 at different temperatures

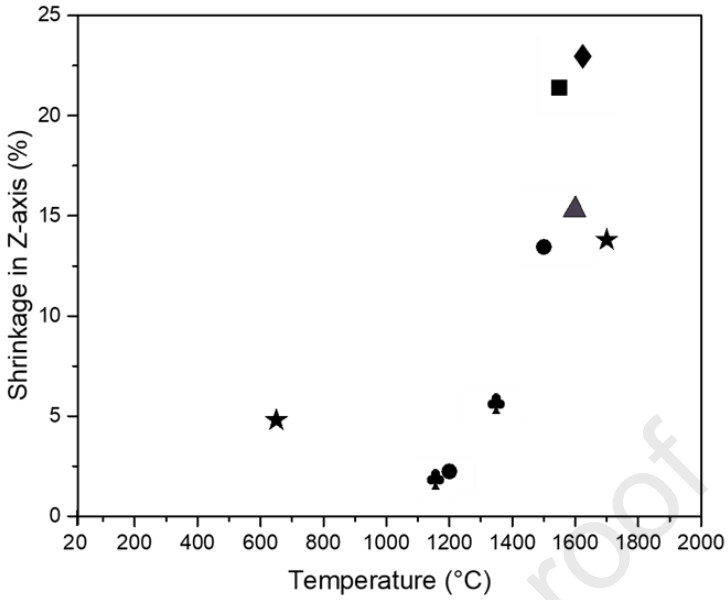

Fig. 11. % Shrinkage comparison of the Z-axis between (♦) Tsui, L.*et al* (2018)[24], (■) Su, B. *et al.* (2008)[23], (▲) Gonzalez, J. A. *et al*. (2016)[31], (●) Liu, Y. *et al*. (2020)[32], (♣) Li, H. *et al.* (2020)[33], and (★) this work.

Highlights

- High solid loaded alumina pastes from 75 to 79.87 wt% were printed by robocasting using PVA, ISOBAM 104 and glycerol as additives.
- The printability of the pastes was achieved using around 1.6 wt% of glycerol, PVA and without the addition of ISOBAM 104.
- The best printability with a high solid load of 79.37 wt% (63.5 vol%) was reached with an [Al] =$1.085x10^{-4}$ M.
- A piece heated at 1700 °C was successfully obtained with a 79.37 wt% of Al_2O_3 and a % shrinkage of 8, 6.8 and 13.8 in X, Y and Z, respectively was reached.

Declaration of interests

☒ The authors declare that they have no known competing financial interests or personal relationships that could have appeared to influence the work reported in this paper.

☒The authors declare the following financial interests/personal relationships which may be considered as potential competing interests: